

Detection of Ground Hazards of El Mokattam Plateau, East Cairo (Egypt), using Terrestrial Laser Scanning

Bassam M. Abdellatif

Data Reception, Analysis and Receiving
Station Affairs Division.
National Authority for Remote
Sensing and Space Sciences (NARSS),
Cairo, Egypt
Email: abdelatif.bassam [AT] gmail.com

Ayman H. Nasr

Data Reception, Analysis and Receiving
Station Affairs Division.
National Authority for Remote
Sensing and Space Sciences
(NARSS),
Cairo, Egypt

Safaa M. Hassan

Data Reception, Analysis and Receiving
Station Affairs Division.
National Authority for Remote
Sensing and Space Sciences (NARSS),
Cairo, Egypt

Abstract— Some catastrophic disasters may be initiated by topographical changes. Rock-fall and landslide are two examples of this type of disasters where information is considered especially scarce. Many places in Egypt are known for these types of topographical changes, such as El Mokattam plateau areas. In this paper Terrestrial Laser Scanning (TLS) technology has been used as an accurate way to predict rock-fall and landslide and produced detailed three dimensional (3D) models of topography in El Mokattam plateau. We evaluate the potential catastrophic movements and landslides as well as delineate the risk zones using 2D and 3D change detection methods. The plateau was scanned during the period between December, 2012 and October, 2013. The scanned cloud points were used to identify the hazard zones and the extent of landslide phenomena in the region. Three different methods; the Ordinary method of slices, Spencer method and Bishop's Simplified method were performed to calculate the factor of safety of slope failures, for determining landslide susceptibility, hazard, and the expected risk. This study shows that with LiDAR monitoring, precursors to rock slope failures, can be identified allowing for better rock slope hazard management by focusing attention on areas with the highest probability of failure.

Keywords-- Terrestrial Laser Scanning; LIDAR; Rock-fall; Landslide; Slope Monitoring.

I. INTRODUCTION

Natural hazards, such as rock-fall and landslide are physically based natural slope [1], they can imperil the infrastructures as well as the populations. Thus, geologists have to remotely assess structural settings and kinematic analysis in order to estimate potential sliding mechanisms. Rock-fall and landslide disasters become major obstacles in development process because their economic losses are relatively high[2]. Unlike the rock-fall, fast downward movement of rocks, or unconstrained course materials, the landslides of slopes and hillsides are mass movements by sliding or flowing under wet conditions. They have caused some major accidents with enormous numbers of

fatality rate all over the world. Generally, there are different factors that cause the catastrophic landslides and rock-fall, e.g. earthquakes, rainfalls, volcanic eruptions, tectonics, mechanical stress changes caused by disturbances or sliding, temperature changes, hydrostatic or hydrodynamic pressures, and loading by trees or anthropogenic changes. In Egypt, reasons of landslides and rock-falls are still a matter of controversy, where this area has no volcanic activities, and earthquakes are not active. However, the movement processes of blocks may occur by detachment of rocks as rock-fall and topples. Also, clay minerals are the weakest of all minerals when saturated by water and act as grazing surface for the overlying blocks[3]. During last decades, new applications in remote sensing and monitoring techniques have been developed and are currently used for natural hazards assessment. More particularly, the acquisition of TLS point clouds usually allow a better understanding of these hazards and greatly facilitate the production and the update of their maps by surveying the same area in successive time periods. Hazard assessment have promoted by the use of photogrammetry and LiDAR. They can provide high resolution and high accuracy 3D point cloud representations of a slope, while eliminating worker exposure to hazard[4] [5]. Furthermore, comparisons of LiDAR data collected over successive time periods allows for the quantification of rock-falls, identification of source areas, quantification of rock-fall history and the calculation of failure probability[6][7][8]. Additionally, monitoring pre-failure deformation of landslides has been conducted with ground based remote sensing technologies such as Terrestrial Laser Scanning (TLS) [9] [10] with combined stereo photogrammetry and aerial LiDAR approaches [11], with satellite interferometric synthetic aperture radar (SAR) [12] [13], and ground based interferometric synthetic aperture radar (GB InSAR) [14] [15].

Rock slope failures are frequently lead by a period of progressive deformation, and brittle fracture damage [16] and this can be detected as surface or subsurface displacements[17]

and precursory rock-falls along fractures defining the eventual failure scar [18]. These processes tend to accelerate prior to failure[19] and this is the basis for failure time prediction [20][21][22]. Monitoring deformation has also been conducted to better understand the mechanisms of landslide failure and its stability state, to design appropriate mitigation measures, and to understand its sensitivity to environmental triggers [23]. Recent efforts using LiDAR monitoring have studied the potential to predict future failure locations and failure time by studying spatial and temporal patterns of precursory activity[24].

TLS is the ideal instrumentation with an exceptional resolution to be used for estimating various parameters, such as: height, aspect, volume, and slope, very accurately. For slope monitoring, it provides a density of data that allows unprecedented visualization for both the overall slope as well as individual sections of the slope. The TLS system used in this study (Optech ILRIS 3D time-of-flight) is comprised of high-resolution digital photography and a laser-based technology called, Light Detection and Ranging (LIDAR). It works something like RADAR, but instead of transmitting radio waves, it transmits laser light pulses. The light bounces off objects and scatters. A telescope receives the backscattered light and a sensitive detector measures the intensity. In addition, from the distance and the orientation of the laser pulse, the xyz coordinates associated with each reflected pulse can be determined. The number of the measured points (cloud points) per square meters varies based on the sensor characteristics, the distance from the target and terrain geometry[25]. Using the acquired data which contain information about shape, distance, measurements, a computer can produce an accurate 3D image. The precise measurements of the dimensions could be used to quantify damages, (e.g. assess landslides and rock-falls). In this paper we present a case study of rock-falls and landslide monitoring in El Mokattam plateau; a fast and accurate

methodology to determine if the slope/fracture is moving or not, calculate the factor of safety using terrestrial LiDAR data.

II. STUDY AREA AND DATA ACQUISITION

El Mokattam plateau, east Cairo-Egypt, lies between Lat. $30^{\circ} 1' 55.48''$ - $30^{\circ} 1' 47.78''$ N and Long $31^{\circ} 16' 43.52''$ - $31^{\circ} 16' 23.83''$ E, as shown in figure 1. Its surrounding edges consist of cliffs which form the side walls of the plateau. It is characterized by steep slope, up to 80° , and appears as sequences of limestone, shale and marl. In the case of significant change, rock masses and fragments of various sizes may fall to the bottom of the plateau by gravity which may cause serious risks to people and housing areas. Potential movement of rocks in certain areas is related to several reasons, including: existence of competent sandstones underlain by incompetent shales, dissection of the coherent cap rock due to intersection of vertical joint sets and bedding planes, presence of exposures with steep slopes, rainfall, and human activities (e.g. mining works, sewage water, and irrigation).

The used scanner was operated in high-speed mode (up to 125,000 points per second) and its internal inclination sensor was utilized to extract leveling information (roll and pitch) for each scan position. It has 1550 nm wavelength, maximum range close to 1.5 kilometer at 80% reflectivity, distance accuracy of 7 mm at 100 m, position accuracy of 8 mm at 100 m, and an angular accuracy of 0.00115 degrees, [26]. Figure 2 (a) represents the TLS position using Google earth satellite 3D image, while (b & c) depict images of the pilot scanned areas outlined in red boxes acquired on December, 2012 and October, 2013, respectively.

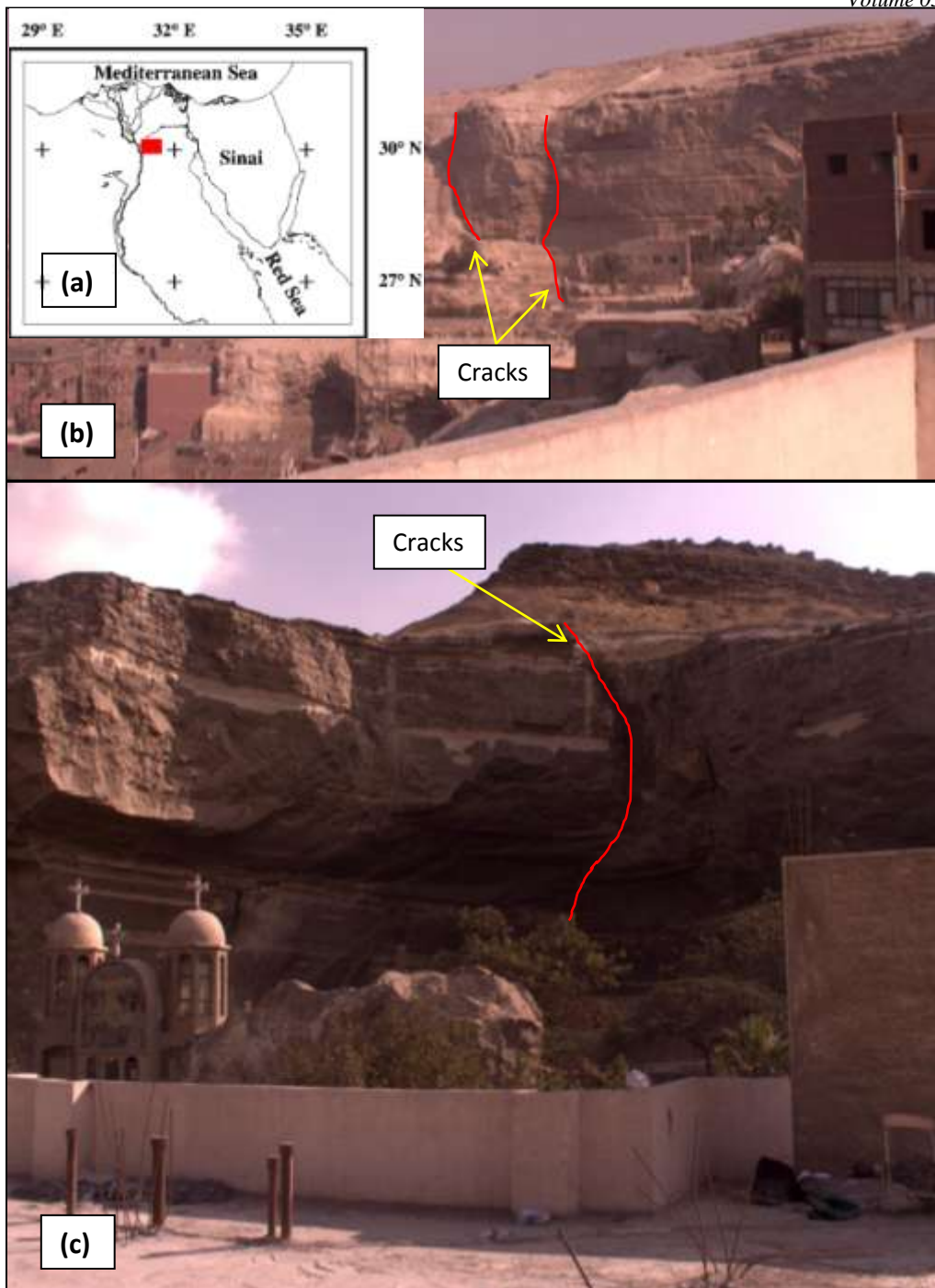


Figure 1. (a) Location map of El Mokattam area, (b, c) Joints/Cracks and steep slope Plateau of the study area

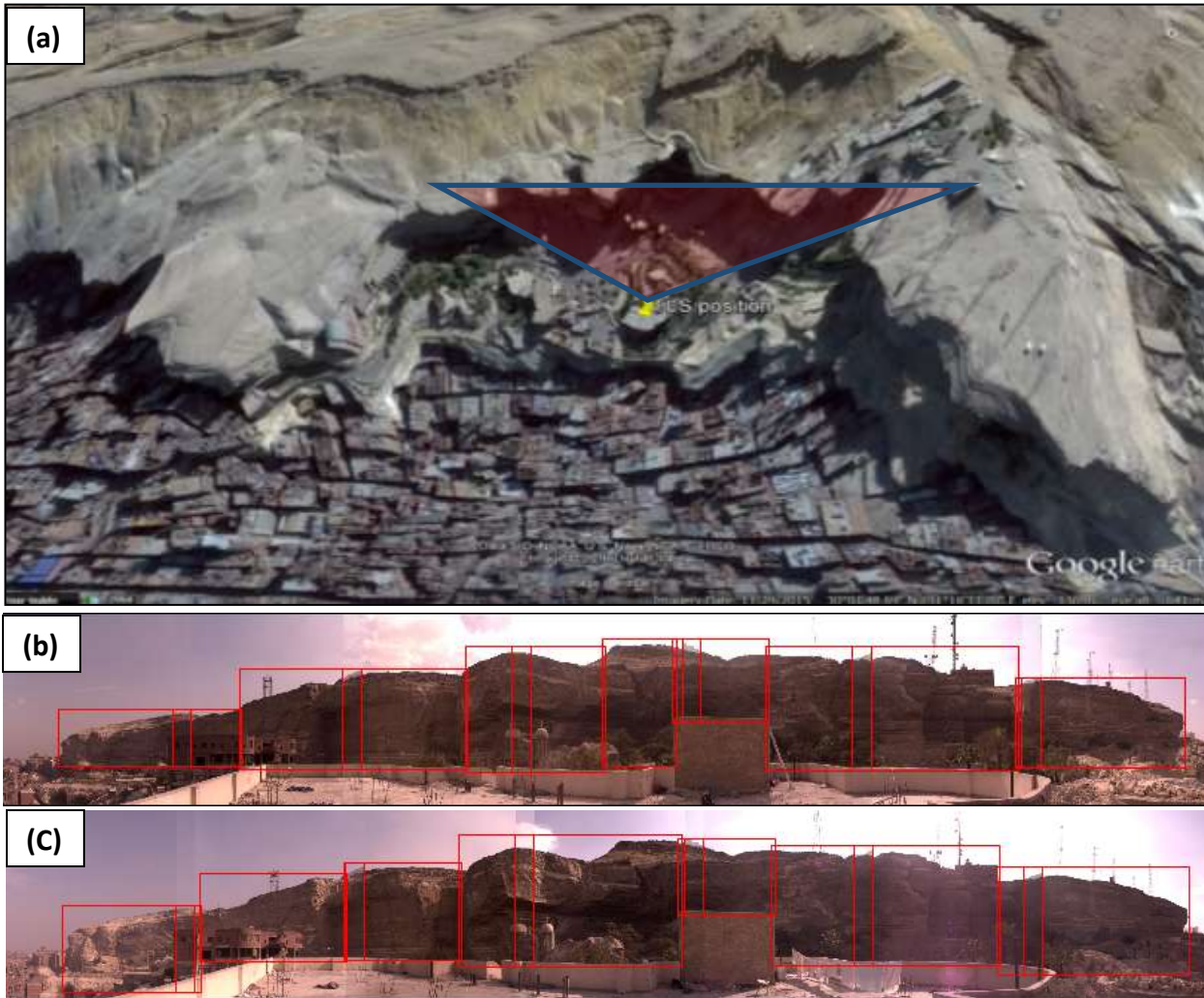


Figure 2. (a) Google earth satellite 3D image of El Mokattam plateau showing the position of the TLS. (b& c) The scan areas in 2012 and 2013 respectively (the red boxes show the different scan tasks)

III. METHODOLOGY

The method of aligning the scans from different dates is to properly geo-reference both data sets. This would save time in the field and during processing. A common processing technique for evaluating the scanned data is the Iterative Closest Point (ICP) technique [27]. This technique compares points from overlapping scan scenes to align these scenes with one another. There are both iterative and non-iterative utilized versions of this technique[28]. However, this technique usually needs a large amount of data and it suffers from accuracy issues as well. One of the most commonly used ICP techniques

come from [29]. This technique does not always converge to an optimal solution [30]. A neighborhood search based approach has also been used for ICP processing [31], and other techniques involve image data as a supplement to scan data[32]. Because of the inherent weakness of ICP, a manual registration technique has been used. One of its advantages is that, it allows the operator to exercise judgment and select scan area components for local geo-referencing that are deemed reliable. After scanning the data in the proposed study area, they need to be locally geo-referenced.

The process of the local geo-referencing is very similar to registration, and is given mathematically by the following equation:

$$\begin{bmatrix} x_{k,j}^{g,reg} \\ y_{k,j}^{g,reg} \\ z_{k,j}^{g,reg} \end{bmatrix} = R(\theta_{s,j}^{g,reg}, \mu_{s,j}^{g,reg}, \psi_{s,j}^{g,reg}) \begin{bmatrix} x_k^{s,j} \\ y_k^{s,j} \\ z_k^{s,j} \end{bmatrix} + \begin{bmatrix} x_t \\ y_t \\ z_t \end{bmatrix}^{g,reg} \quad (1)$$

Where $x_k^{s,j}$, $y_k^{s,j}$ and $z_k^{s,j}$ are the coordinates (x, y and z) for each point k in the local scan coordinates s, j. Note that j is the scan number (in this case “1” or “2”) for the two dates. Also, $x_{k,j}^{g,reg}$, $y_{k,j}^{g,reg}$ and $z_{k,j}^{g,reg}$ are the scan data in the global coordinates (g, reg) in x, y and z after they have been translated and rotated as outlined in equation (1). Scans from both dates are put into coordinates $x_{k,j}^{g,reg}$, $y_{k,j}^{g,reg}$ and $z_{k,j}^{g,reg}$; this coordinate frame ensures that both scan data sets are locally geo-referenced so appropriate slope motions can be found. To rotate the scanned data from coordinate frame s, j to g, reg, the rotation matrix $R(\theta_{s,j}^{g,reg}, \mu_{s,j}^{g,reg}, \psi_{s,j}^{g,reg})$ is used. The rotation matrix is a function of three rotations about the x, y and z axes: $\theta_{s,j}^{g,reg}$, $\mu_{s,j}^{g,reg}$, and $\psi_{s,j}^{g,reg}$, respectively. The use of rotation matrices in this manner is well established [33] [34]. For translation along the x, y and z axes, the terms x_t , y_t and z_t are utilized, respectively.

Usually, the previous equation can be solved given targets appearing in both scan scenes and a least square solution [35] [36]. For targets to be useful, they should be placed far enough apart so that accurate angular information can be obtained. Ideally, targets should be normal to the laser scanner beam. Without targets, building features can be used as substitutes. Scanning was conducted at a suitable distance from the plateau. The point clouds were produced using the manufacture software, as illustrated in figure 3 (a & b). Due to several numbers of smaller scans, different tilting and vertical angles, and the cloud points of the natural scene that exposed to movement events between the 2 scanning dates, building surrounding the scanner position (assumed as nonmoving objects) were used for the processing carried out. To do this, the roof of the building where the scanner has been installed, the church domes and other man-made objects were selected from the point clouds. Then, scans were manually moved until the same features were properly aligned. Using the previously outlined local registration technique, it was possible to achieve good accuracy of about 0.15 m. This is considered acceptable given that the used sensor accuracy is 0.07m at 100 m. Figure 4 illustrates the top view of the scanned area before and after being aligned. The next step after registration is to calculate the changes between the two point clouds within the 11 months’ time period.

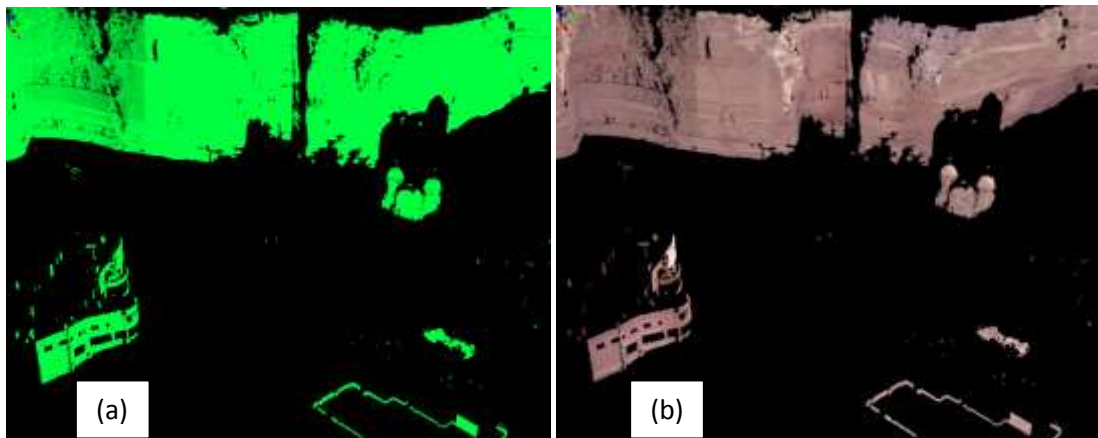


Figure 3. (a) The study area buildings with significant features used for Local Geo-referencing using cloud points, (b) RGB images draped on the cloud points.

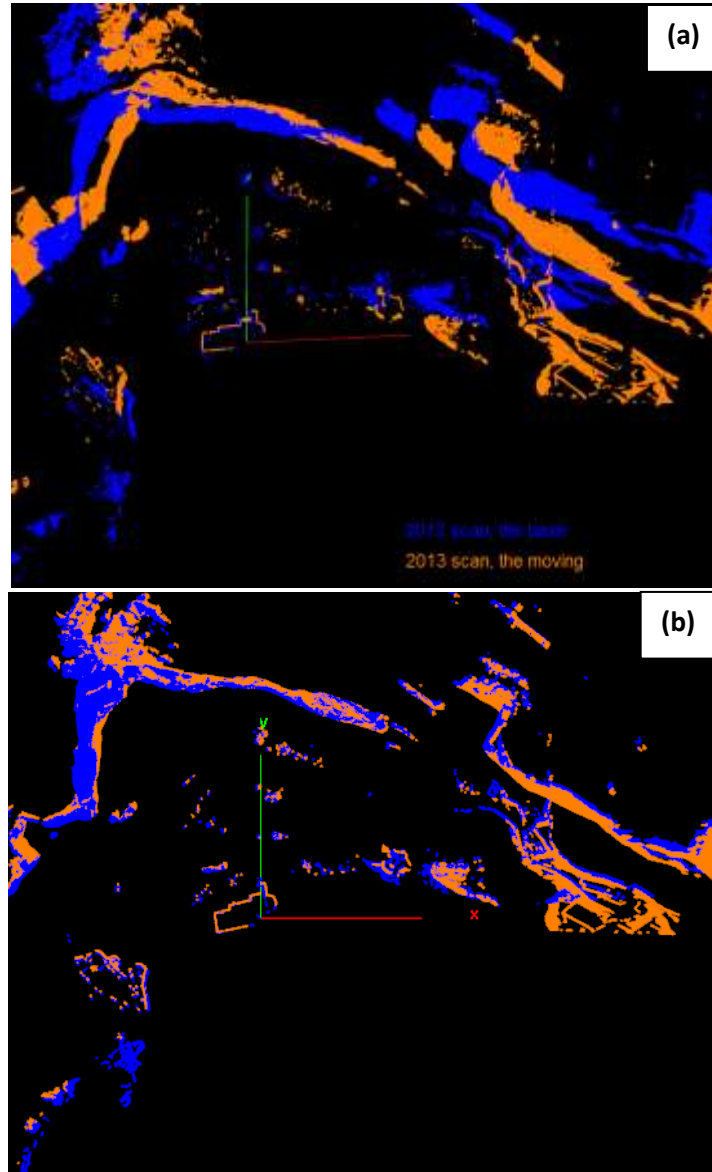


Figure 4. Top view of the scanned areas in (2012 & 2013) (a) before and (b) after being aligned

IV. RESULTS AND DISCUSSION

The total number of scan points was 71, 615, 292 and 87, 238, 471, for the October, 2012 and December, 2013 scans, respectively. This was considered as a sufficient number of points to undertake this research. Overall deformations of the slope for the two scanned dates are shown in figure 5. Most of changes lay in the range from 0 to 0.15 m. This range considered as registration error between the two data sets. Therefore, no displacement was identified between the two dates except for the new construction activities and for objects

that are not found simultaneously in the two images. Nevertheless, the observed cracks at the left and the middle parts of the plateau may increase the failure risk probability. Some localized failures and surface tension cracks were already observed in the field (Figure 1). Therefore, many vertical cross sections have been tested through El Mokatam plateau as shown in figure 6. Only two of them (P04 & P10) representing the overall probability of the landslide in 2D are depicted in figures (7, 8 - (a)). Figures (7, 8 - (b)) illustrate, the plan view of their point cloud's data.

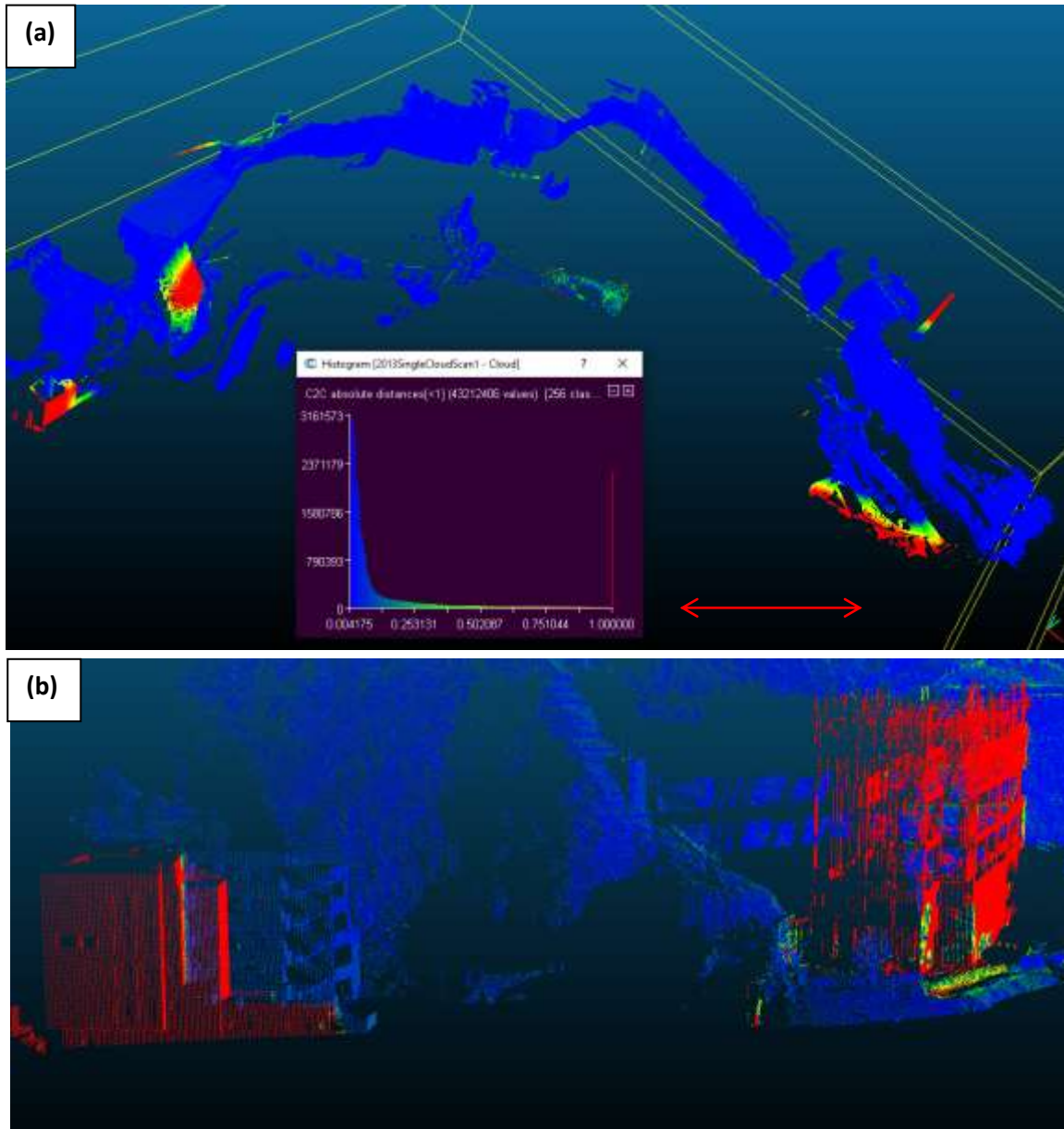


Figure 5. (a) Slope deformations for the two scanned dates (Oct, 2012 and Dec, 2013). (b) New constructed buildings are colored in red in the change map.

The SLOPE/W was used to create a simple slope stability analysis for these cross sections. The soil layer was modeled using its Limit Equilibrium Methods (LEM); the Ordinary

method of slices, Spencer method and Bishop's Simplified method [37]. Figures (7, 8 - (c)) depict the output of the Ordinary method of slices.

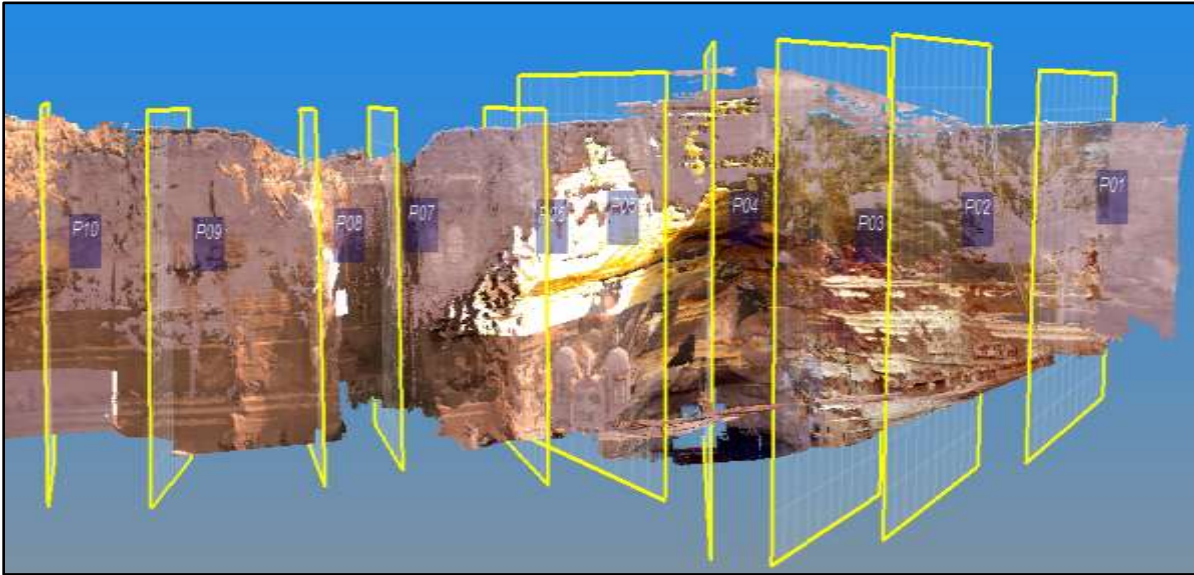


Figure 6. RGB images draped on the cloud points data showing the distribution of ten cross sections (P01 - P10) through El Mokattam plateau.

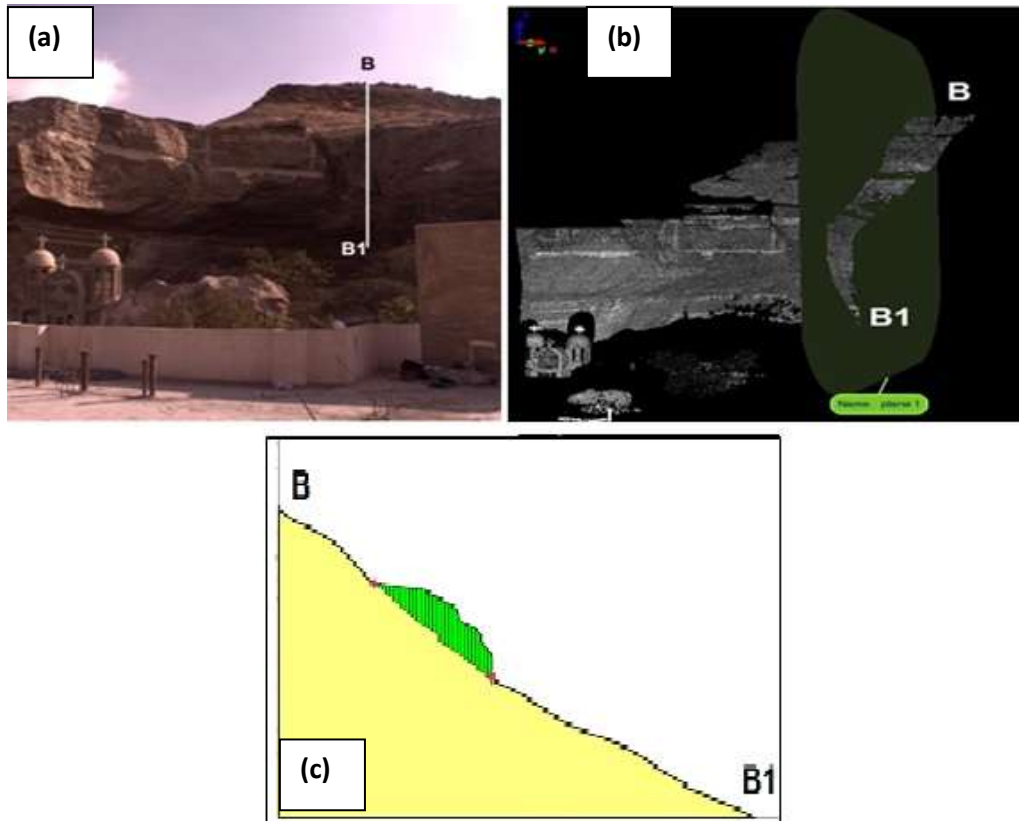


Figure 7. (a) Field photo showing the BB1 cross section (P04) using scan task1, (b) The BB1 cross section on the point cloud data, (c) SLOPE/W representation of the slope at the cross section

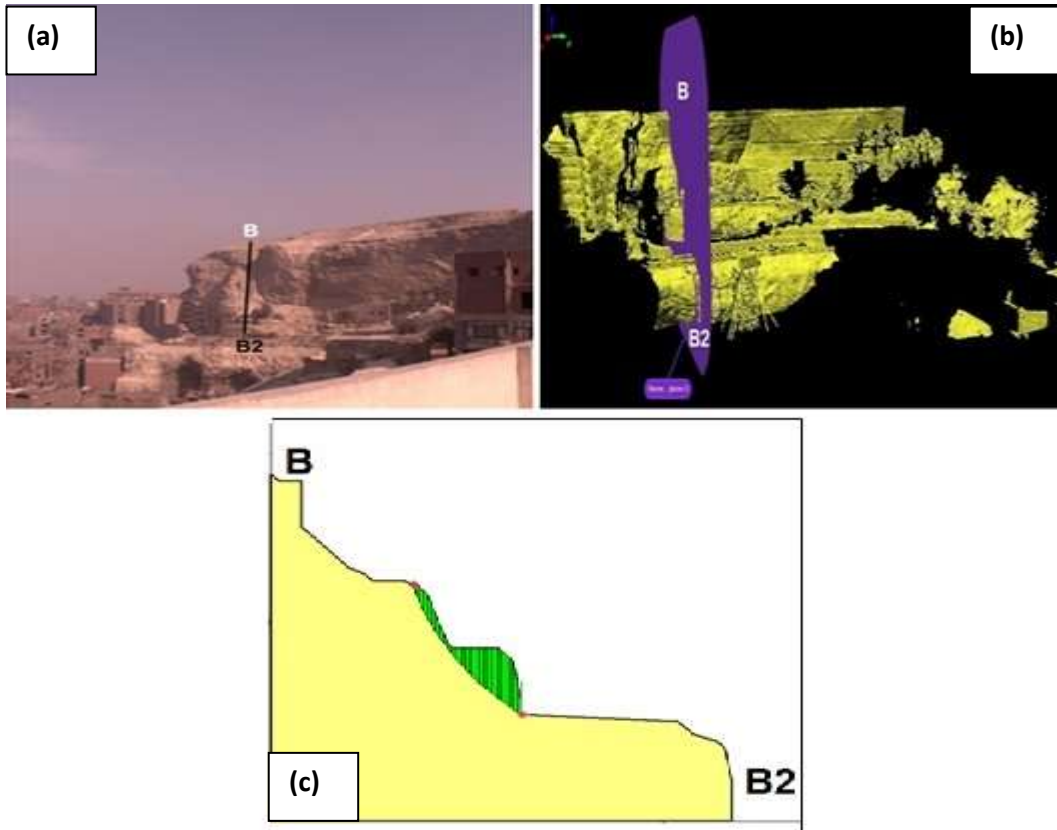


Figure 8. (a) Field photo showing the BB2 cross section (P10) using scan task2, (b) The BB2 cross section on the point cloud data, (c) SLOPE/W representation of the slope at the cross section.

As there was no information about the variation of geologic parameters in the vertical direction, linear-elastic behaviour is considered. The green color shaded area represents the sliding surface area. The residual friction angle obtained by this analysis is 27.9° . The factors of safety values obtained by the different LEM methods, at this particular friction angle value, are given in table 1. It shows that the affected area at El Mokattam plateau located in scan-task 2 is higher in risk than that of scan-task 1 according to equation (2) due to the cracks affecting this area.

Table 1. Factor of safety calculated for the two vertical cross sections representing the overall probability of the landslide using three different methods

Location	Factor of Safety Methods		
	Ordinary	Spencer	Bishop's Simplified
Scan-task 1	1.005	1.005	1.007
Scan-task 2	0.654	0.654	0.661

V. CONCLUSION

A study of the Mokattam plateau, east Cairo (Egypt) is carried out using Terrestrial Laser Scanner (TLS). It demonstrates its advantages in the assessment of rock-fall and landslide hazards and the topographic change monitoring over certain period. It enabled us to model the accurate surface geomorphology and capture the existent geometry. This study was conducted mainly to investigate and calculate the stability of different hazard areas. A comparison of the stability values at different cross sections in 2D LEM (Ordinary, Bishop's Simplified and Spencer's methods) was performed. The following conclusions are based on the 2D slope stability analysis:

1. A variation of the factor of safety values is observed with 2D LEM different analysis methods.
2. The increase in the stability value has a stabilizing effect on the landslide.

3. There are two zones (scan-task1) and (scan-task2) have higher deformation rates and spatial extension than the others.
4. The deformation areas lies exactly on the tectonic fracture zone observed during the field work.
5. The high resolution, accuracy and the maximum range of the TLS offered interesting prospects for both spatial location and deformation.
6. Detection of precursory events for smaller magnitude rock-falls would require higher spatial resolution. For especially active and high risk sites, continuous monitoring may be a viable monitoring tool providing early warning of rock-falls.

REFERENCES

- [1] L.C., Hengxing, M., Derek, Z., Chenghu; and H. L., Chang, Rockfall hazard analysis using LiDAR and spatial modeling”. *Geomorphology* 118, 2010, pp. 213–223.
- [2] F., Guzzetti, A. C., Mondini, M., Cardinali, F., Fiorucci, M., Santangelo, and K. T., Chang, Landslide inventory maps: New tools for an old problem”. *Earth-Science Reviews* 112, 2012, pp. 42–66.
- [3] F.G.H. Blyth and M.H., de Freitas, A geology for engineers”. Edward Arnold, London. Sixth Ed. 1974.
- [4] M.J., Lato, D.J., Hutchinson, D., Gauthier, T., Edwards, M., Ondercin, Comparison of ALS, TLS and terrestrial photogrammetry for mapping differential slope change in mountainous terrain. *Can. Geotech. J.* <http://dx.doi.org/10.1139/cgj-2014-0051>.
- [5] R. A., Kromer, D. Jean Hutchinson, Matt J. Lato, Dave Gauthier, Thomas Edwards, Identifying rock slope failure precursors using LiDAR for transportation corridor hazard management”. *Engineering Geology* 195, 2015, pp. 93–103.
- [6] A., Abellán, J.M., Vilaplana, J., Calvet, D., García-Sellés, E., Asensio, “Rockfall monitoring by Terrestrial Laser Scanning —case study of the basaltic rock face at Castellfollitde la Roca (Catalonia, Spain)”. *Nat. Hazards Earth Syst. Sci.* 11, 2011, pp. 829–841. <http://dx.doi.org/10.5194/nhess-11-829-2011>.
- [7] D., Santana, J., Corominas, O., Mavrouli, D., Garcia-Sellés, Magnitude–frequency relation for rockfall scars using a Terrestrial Laser Scanner. *Eng. Geol.* 2012, pp. 145–146, 50–64. <http://dx.doi.org/10.1016/j.enggeo.2012.07.001>.
- [8] T., Dewez, J., Rohmer, V. Regard, and C., Cnudde, Probabilistic coastal cliff collapse hazard from repeated terrestrial laser surveys: Case study from Mesnil Val (Normandy, northern France), *Journal of coastal research*, 2013.
- [9] A., Abellán, J., Calvet, J.M., Vilaplana, J., Blanchard, “Detection and spatial prediction of rockfalls by means of terrestrial laser scanner monitoring”. *Geomorphology* 119, 2010, pp. 162–171. <http://dx.doi.org/10.1016/j.geomorph.2010.03.016>.
- [10] T., Oppikofer, M., Jaboyedoff, L., Blikra, M.H., Derron, R., Metzger, Characterization and monitoring of the Åknes rockslide using terrestrial laser scanning. *Nat. Hazards Earth Syst. Sci.* 9, 2009, pp.1003–1019. <http://dx.doi.org/10.5194/nhess-9-1003-2009>.
- [11] O., Dewitte, J.C., Jasselette, Y., Cornet, M., Van Den Eeckhaut, A., Collignon, J., Poesen, A., Demoulin, “Tracking landslide displacements by multi-temporal DTMs: a combined aerial stereo photogrammetric and LIDAR approach in western Belgium”. *Eng. Geol.* 99, 2008, pp. 11–22. <http://dx.doi.org/10.1016/j.enggeo.2008.02.006>.
- [12] Z., Perski, R., Hanssen, A., Wojcik, T., Wojciechowski, InSAR analyses of terrain deformation near the Wieliczka Salt Mine, Poland. *Eng. Geol.* 106, 2009, pp. 58–67. <http://dx.doi.org/10.1016/j.enggeo.2009.02.014>.
- [13] P., Vallone, M.S., Giammarinaro, M., Crosetto, M., Agudo, E., Biescas, Ground motion phenomena in Caltanissetta (Italy) investigated by InSAR and geological data integration”. *Eng. Geol.* 98, 2008, pp. 144–155. <http://dx.doi.org/10.1016/j.enggeo.2008.02.004>.
- [14] F., Bozzano, I., Cipriani, P., Mazzanti, A., Prestininzi, Displacement patterns of a landslide affected by human activities: insights from ground-based InSAR monitoring. *Nat. Hazards* 59, 2011, 1377–1396. <http://dx.doi.org/10.1007/s11069-011-9840-6>.
- [15] V., Gischtig, S., Loew, A., Kos, J.R., Moore, H., Raetzo, F., Lemy, Identification of active release planes using ground-based differential InSAR at the Randa rock slope instability, Switzerland. *Nat. Hazards Earth Syst. Sci.* 9,

- 2009, pp. 2027–2038, <http://dx.doi.org/10.5194/nhess-9-2027-2009>.
- [16] Stead, D., Eberhardt, E., Coggan, J.S., “Developments in the characterization of complex rock slope deformation and failure using numerical modelling techniques”. *Eng. Geol.* 83, 2005, pp. 217–235, <http://dx.doi.org/10.1016/j.enggeo.2005.06.033>.
- [17] M.-G., Angeli, A., Pasuto, S., Silvano, “A critical review of landslide monitoring experiences”. *Eng. Geol.* 55, 2000, pp. 133–147. [http://dx.doi.org/10.1016/S0013-7952\(99\)00122-2](http://dx.doi.org/10.1016/S0013-7952(99)00122-2).
- [18] N., Rosser, M., Lim, D., Petley, S., Dunning, R., Allison, Patterns of precursory rockfall prior to slope failure. *J. Geophys. Res.* 112, F04014. <http://dx.doi.org/10.1029/2006JF000642>.
- [19] R. Nishii, and N., Matsuoka, Monitoring rapid head scarp movement in an alpine rockslide. *Eng. Geol.* 115, 2010, pp. 49–57. <http://dx.doi.org/10.1016/j.enggeo.2010.06.014>.
- [20] T., Fukuzono, Recent studies on time prediction of slope failure. *Landslide News* 4 (9), 1990.
- [21] G.B. Crosta, and F., Agliardi, How to obtain alert velocity thresholds for large rockslides. *Phys. Chem. Earth A/B/C* 27, 2002, 1557–1565. [http://dx.doi.org/10.1016/S1474-7065\(02\)00177-8](http://dx.doi.org/10.1016/S1474-7065(02)00177-8).
- [22] D.N., Petley, The evolution of slope failures: mechanisms of rupture propagation. *Nat. Hazards Earth Syst. Sci.* 4, 2004, pp. 147–152. <http://dx.doi.org/10.5194/nhess-4-147-2004>.
- [23] E., Eberhardt, A., Watson, S., Loew, Improving the interpretation of slope monitoring and early warning data through better understanding of complex deep-seated landslide failure mechanisms. *Landslides and engineered slopes. From the past to the future. Proceedings of the 10th International Symposium on Landslides and Engineered Slopes*, 30 June–4 July 2008, Xi'an, China. CRC Press, 2010, pp. 39–51, <http://dx.doi.org/10.1201/9780203885284-c3>.
- [24] M.J., Royán, A., Abellán, M., Jaboyedoff, J.M., Vilaplana, J., Calvet, Spatio-temporal analysis of rockfall pre-failure deformation using Terrestrial LiDAR. *Landslides* 11, 2013, pp. 697–709. <http://dx.doi.org/10.1007/s10346-013-0442-0>.
- [25] K. A., Razak, M. W., Straatsma, C. J., van Westen, J. P. Malet, and S.M., de Jong, Airborne laser scanning of forested landslides characterization: terrainmodel quality and visualization. *Geomorphology* 126, 2011, pp. 186–200.
- [26] Optech, 2009: “ILRIS Laser Scanner, Data Sheet”.
- [27] N., Gelfand, L., Ikemoto, S., Rusinkiewicz, and M., Levoy, Geometrically stable sampling for the ICP algorithm, *Proc. International Conference on 3D Digital Imaging and Modeling*, 2003.
- [28] J. Y., Han, A non-iterative approach for the quick alignment of multi-station unregistered LiDAR point clouds”. *IEEE Geoscience and Remote Sensing Letters*, Vol. 7, No. 4, 2010.
- [29] P., Besl, and N., McKay, A method for registration of 3D shapes. *Institute of Electrical and Electronics Engineers (IEEE) Transactions on Pattern Analysis and Machine Intelligence*, 14 (2), 1992, pp. 239-256.
- [30] K. H., Bae, Automated registration of unorganized point clouds from terrestrial laser scanners”. PhD thesis, Department of Spatial Sciences, Curtin University of Technology, Perth, Australia, 2006.
- [31] K.H. Bae, and D.D., Lichti, A method for automated registration of unorganized point clouds”. *ISPRS Journal of Photogrammetry and Remote Sensing*, 63 (1), 2008, pp. 36-54.
- [32] C. Dold, and C., Brenner, Registration of Terrestrial Laser Scanning Data Using Planar Patches and Image Data”. *ISPRS Commission V Symposium on Image Engineering and Vision Metrology*, 2006, pp. 78-83.
- [33] G., Arfken, “Mathematical Methods for Physicists”, 3rd ed. Orlando, 1985, FL: Academic Press.
- [34] H., Goldstein, *Classical Mechanics*, 2nd ed. Reading, MA: Addison-Wesley, 1980.
- [35] D.E., Wells, E.J., Krakiwsky, *The Method of Least Squares, Lecture Notes*, Depart of Geodesy and Geomatics Engineering, University of New Brunswick, 1971, pp. 192.
- [36] Wolf and Ghilani, “Adjustment Computations: Statistics and Least Squares in Surveying and GIS”. John Wiley and Sons, 1997, pp. 584.
- [37] J., Krahn, *Stability Modeling With SLOPE/W* [M]. Canada: GEO-SLOPE/W International Ltd, 2004.